Force Field Optimization for Organic Mercury Compounds

M. H. Lagache,[†] J. Ridard,[†] P. Ungerer,*[,†,‡] and A. Boutin[†]

Laboratoire de Chimie Physique, Université de Paris Sud, UMR 8000 CNRS, 91405 Orsay Cedex, France, and Institut Français du Pétrole, 1-4 avenue de Bois Préau, 92852 Rueil Malmaison Cedex, France

Received: January 22, 2004; In Final Form: April 19, 2004

Organic mercury compounds can be found in petroleum and natural gas products in very small concentrations. The knowledge of the thermodynamic properties of these compounds is important for the petroleum industry. Among the thermodynamic properties useful for industry, the solubilities of organic mercury compounds such as dimethylmercury ($Hg(CH_3)_2$) and diethylmercury ($Hg(C_2H_5)_2$) in organic or aqueous solvents are important to be determined. Since experiments are difficult to perform due to the very high toxicity of these molecules, we developed a force field including electrostatic interactions to be able to obtain these properties by molecular simulation. Our results are in good agreement with the experimental data and also show a weak influence of the electrostatic part in the potential. This force field development enables us to obtain liquid−vapor equilibrium of mercury compound−light alkane mixture.

1. Introduction

Molecular simulation continues to be applied more and more in chemical engineering because it is a feasible route to evaluate thermodynamic properties of realistic systems as a consequence of the increase of computer power at moderate cost. It is especially considered when little experimental information is available as in the case of the organic mercury compounds. In addition to their poisoning of industrial catalysts, these compounds damage aluminum alloy heat exchangers and pipelines by corrosion and present a health risk for operators. For this reason, the knowledge of the thermodynamic properties of these compounds and particularly dimethylmercury ($Hg(CH_3)_2$) and diethylmercury ($Hg(C_2H_5)_2$) is important for the petroleum industry.[1−4] Since experiments are difficult to perform due to the high toxicity of these molecules, Monte Carlo simulations are of great interest to determine their thermodynamic properties. The aim of this work is to develop a complete force field, including bonded and nonbonded (van der Waals and electrostatic) interactions, following works on thiols[5] and aldehydes and ketones.[6]

The electrostatic part of the intermolecular potential is represented by a set of point charges obtained by fitting the molecular electrostatic potential (see for instance refs 7 and 8), and the repulsion-dispersion part is represented by a Lennard-Jones potential. For the CH_3 and CH_2 groups, we have used the Anisotropic United Atoms potential (AUA4) of Ungerer et al.[9] which leads to accurate predictions of equilibrium properties of a large range of *n*-alkanes. Compared with more classical United Atoms potentials for alkanes, AUA potentials use the same groups (CH_3, CH_2,...), but the Lennard-Jones force center is shifted to an intermediate position between the carbon and hydrogen atoms of the related group instead of being placed on the carbon nucleus.

It is well-known that alkanes do not present a significant permanent dipole moment, thus the AUA4 parameters were determined without using electrostatic energetic contribution. In the case of mercury compounds we have studied in detail the electrostatic interactions. The electrostatic models could be necessary when simulating mixtures with polar solvents in the future. However for pure organic mercury liquid, the electrostatic interaction has been found to be very small, and the Lennard-Jones parameters of the mercury atom have been optimized without electrostatic interactions to reproduce the few thermodynamical experimental data available in the literature.[10−12]

The paper is organized as follows. In section 2, the analytical form of the force field and the optimization procedure are presented. Section 3 is devoted to the results concerning the optimization of the geometry of the molecules, the determination of the intramolecular potential (bending and torsion angles), the determination of the electrostatic and the Lennard-Jones potentials, and the calculation of the thermodynamic properties. The corresponding discussion is included in each section.

2. Methods

2.1. Analytical Form of the Force Field. The molecular potential is divided into an intramolecular part and an intermolecular part according to

$$U^{intra} = U^{intra}_{bend} + U^{intra}_{tors} + U^{intra}_{LJ} \quad (1)$$

$$U^{inter} = U^{inter}_{elec} + U^{inter}_{LJ} \quad (2)$$

where U^{intra}_{bend} and U^{intra}_{tors} correspond, respectively, to the variation of the bending angle and of the dihedral angle, and U^{intra}_{LJ} corresponds to nonbonded van der Waals interactions (i.e. interactions between united atoms belonging to the same molecule and separated by more than three chemical bonds). U^{inter}_{elec} represents the electrostatic interactions, and U^{inter}_{LJ} represents the repulsion− dispersion interactions. We did not take into account explicitly the polarization energy.

The bending potential is represented by the harmonic function

$$\frac{U^{bend}(\theta)}{k_b} = \frac{1}{2}k_\theta(\theta - \theta_0)^2 \quad (3)$$

* Corresponding author e-mail: philippe.ungerer@ifp.fr.
† Université de Paris Sud.
‡ Institut Français du Pétrole.

10.1021/jp049676x CCC: $27.50
Published on Web 05/25/2004

where θ is the bond angle (θ_0 being the equilibrium value). We do not use the harmonic bending potential in $\cos(\theta)$ described in ref 13 because the C−Hg−C bending angle equilibrium value is 180°, so that a fitting procedure in $\cos(\theta)$ is not possible. The torsion potential is defined as follows[13]

$$\frac{U^{tors}(\Phi)}{k_b} = \sum_{j=1}^{n} a_j (cos\Phi)^j \tag{4}$$

where Φ is the dihedral angle ($\Phi = 0$ for the trans conformation).

Electrostatic interactions are modeled by a set of point charges $\{q_i\}$

$$U_{elec}^{inter} = \frac{q_i q_j}{r_{ij}} \tag{5}$$

where r_{ij} is the distance between the charge i and the charge j.

Dispersion−repulsion interactions are represented by a chain of Lennard-Jones sites standing for each CH_3 or CH_2 group and for mercury atom. The interactions take place between two united atoms, i and j, of different molecules according to the following formula:

$$\frac{U_{LJ}^{inter}}{k_b} = -4\epsilon_{ij}\left(\frac{\sigma_{ij}^6}{r_{ij}^6} - \frac{\sigma_{ij}^{12}}{r_{ij}^{12}}\right) \tag{6}$$

Lorentz−Berthelot combining rules are used to determine the parameters for unlike group interactions:

$$\epsilon_{ij} = \sqrt{\epsilon_{ii}\epsilon_{jj}} \tag{7}$$

$$\sigma_{ij} = \frac{1}{2}(\sigma_{ii} + \sigma_{jj}) \tag{8}$$

2.2. Optimization Procedure of the Force Field. To optimize the force field, we follow the procedure used for sulfides and thiols[5] and for aldehydes and ketones.[6] The first step consists of determining the intramolecular potential by fit of ab initio molecular energy curves and the point charge distribution by fit of the ab initio electrostatic molecular potential. The second step consists of fitting the parameters of the Lennard-Jones potential on well chosen thermodynamic properties. For each reference compound (dimethylmercury and diethylmercury), we have considered the vapor pressure, the vaporization enthalpy, and the liquid density at temperatures available in the literature. Considering the vaporization enthalpy and the liquid density as reference data allows a reliable extension to lower and higher temperatures since these properties control the temperature dependence of the vapor pressure through the Clapeyron equation. In addition, the vapor pressure is representative of the chemical potential of the liquid phase. A good representation of the vapor pressure ensures that the equilibrium properties are well calculated and that the entropy of the liquid phase is well described. To optimize a given set of parameters, we performed Monte Carlo simulations in two reference states for each compound: one biphasic simulation at a temperature above the boiling temperature and one monophasic simulation at a temperature below the boiling temperature.

The optimization procedure of the Lennard-Jones parameters has already been described in the work of Ungerer et al.[9] and is thus only summarized here. The following dimensionless error criterion is used

$$F(y_1,....,y_m) = \frac{1}{n}\sum_{i=1}^{n}\frac{(X_i^{mod} - X_i^{exp})^2}{s_i^2} \tag{9}$$

where X_i^{mod} is the computed value of the physical property X_i ($\ln(P_{sat})$, ΔH_{vap}, ρ_{liquid}), s_i is the estimated statistical uncertainty on X_i^{mod} (statistical inefficiency estimated from a simulation using the standard block average technique[14]), and X_i^{exp} is the experimental value of X_i. F is considered as a function of two parameters y_j to optimize in the case of mercury atom, namely, $y_1 = \epsilon_{Hg}$ and $y_2 = \sigma_{Hg}$.

The minimization of the error criterion requires the knowledge of derivatives of the computed values versus the parameters. These derivatives are evaluated by finite differences. Care must be taken that the starting point (i.e., the set of initial parameter values) is not too far from the optimum, otherwise the optimization process is unstable.

2.3. Monte Carlo Simulations. The Gibbs ensemble Monte Carlo (GEMC) introduced by Panagiotopoulos,[15] implemented with the configurational bias,[16] was used for liquid−vapor equilibrium simulation. For pure compounds, biphasic simulations were performed above the boiling temperature at constant total volume. For mixtures, biphasic simulations were performed at constant pressure. Monophasic simulations, at constant pressure, were performed in order to investigate pure compounds below the boiling temperature. The various Monte Carlo moves implemented in this study were rigid body translations and rotations, phase volume changes, internal rotations,[17] configurational bias regrowth,[16] and molecule transfers between phases. Move frequencies used for biphasic systems of pure compounds are as follows: for the dimethylmercury, 15% translations, 15% rotations, 0.5% volume changes, and 69.5% transfers; for the diethylmercury, 9.8% translations, 9.8% rotations, 10% internal rotations, 0.4% volume changes, and 70 transfers. For the mixture, move frequencies are as follows: 10% translations, 20% rotations, 9.5% internal rotations, 20% partial regrowth, 0.5% volume changes, and 40% transfers. For monophasic systems, we considered for dimethylmercury, 49% translations, 49% rotations, and 2% volume changes and for diethylmercury, 24.8% translations, 24.8% rotations, 50% internal rotations, and 0.4% volume changes. The total number of molecules used for GEMC at constant volume and NPT simulations was 200 and 300 for the mixture. A cutoff radius of 10 Å was used, together with standard long range corrections.[14] Vapor pressure, molar vaporization enthalpy, and liquid density were computed by averaging after an adequate stabilization period. Vapor pressure was taken as the average pressure evaluated by the virial expression[14] in the vapor simulation box. The molar vaporization enthalpy was computed as the difference between the average molar enthalpies of liquid and vapor simulation boxes. The average liquid density was determined directly as the ratio of the average mass of the liquid simulation box and its volume. These three properties were generally determined with a statistical uncertainty of 5%, 1%, and 0.5%, respectively.

As mentioned in ref 9, the Gibbs ensemble method is poorly efficient for temperature lower than the boiling temperature. To extend the computation of the vapor pressure to lower temperatures, as proposed by Kofke,[18] the Clapeyron equation was integrated, using an integration scheme of second order with regularly spaced $1/T$ values.[9]

$$\ln(P_{sat}(T_{n+1})) = \ln(P_{sat}(T_{n-1})) - \left(\frac{1}{T_{n+1}} - \frac{1}{T_{n-1}}\right)\frac{\Delta H_{vap}(T_n)}{R} \tag{10}$$

TABLE 1: *Ab Initio* Results of Distances and Angles for the Dimethylmercury Compared with the Experimental Determinations of Rao et al.[21]

	ab initio (this work)	experimental[21]
C−Hg distance	2.086 Å	2.094 ± 0.005 Å
C−H distance	1.093 Å	1.09 ± 0.02 Å
C−Hg−C angle	180°	180°
H−C−H angle	109.5°	109.3 ± 1.0°

Below the normal boiling point, the molar vaporization enthalpy was estimated from a single monophasic simulation at constant pressure[9]

$$\Delta H_{vap} \simeq \langle -U_L^{ext} \rangle + RT \qquad (11)$$

where $\langle U_L^{ext} \rangle$ is the average molar intermolecular potential energy of the liquid simulation box.

3. Results and Discussion

3.1. Equilibrium Conformations. The structural parameters of dimethylmercury and diethylmercury were determined at the MP2 level using the GAUSSIAN[19] package. The 6-311G** basis set was used for C and H atoms. The effective core potential SBKJC[20] has been used for the mercury atom, with the associated valence basis set, plus an *f* orbital with exponent 1.13 (this value has been obtained by minimizing the MP2 energy). The results for dimethylmercury are given in Table 1 together with the experimental results (pure rotational Raman spectra) of Rao et al.[21] There is an excellent agreement between the ab initio calculations and the experimental data. Rao et al. assert that the dimethylmercury has a linear structure, and this is confirmed by the ab initio results.

In the case of diethylmercury, no experimental structural data are available. The bond lengths in the dimethylmercury and in the diethylmercury are expected to be close, and, indeed, the C−Hg distance obtained from the present ab initio calculations is 2.094 Å in diethylmercury totally free of moving and 2.086 Å in dimethylmercury. So we optimize the geometry of diethylmercury by constraining the C−Hg distance to be the same as in dimethylmercury. The ab initio C_2-Hg-C_3 and C_1-C_2-Hg bending angles of the diethylmercury are equal to 180° and 113.4°, respectively, and the ab initio $C_1-C_2-C_3-C_4$ supertorsion angle is equal to 137.7°. The term "supertorsion" is explained in the next section.

3.2. Intramolecular Potential. We follow the same procedure for the determination of each part of the intramolecular potential. It consists of constraining all distances and all angles to their equilibrium value except the angle corresponding to the researched potential which varies by regular increment. Then we determine the bending rigidity, k_θ, or the a_j torsion parameters by fitting the appropriate energy curve, calculated at the same level of accuracy as in the preceding section. The results are given in Table 2.

The energy of dimethylmercury as a function of the bending angle C−Hg−C is shown in Figure 1. Fitting this function leads to the following parameters: $k_\theta = 14\,100$ K and $\theta_0 = 180°$. As a result, the half width of the distribution of the bending angle at 293.15 K is approximately 20° (see Figure 2).

Concerning diethylmercury, the bending parameters for the C_1-C_2-Hg angle and for the C_2-Hg-C_3 angle are $k_\theta = 23\,620$ K and $\theta_0 = 113.4°$ and $k_\theta = 17\,140$ K and $\theta_0 = 180°$, respectively. The definition of the torsion of diethylmercury is delicate because when the C_2-Hg-C_3 angle is equal to 180°, the classical dihedral $C_1-C_2-Hg-C_3$ angle is undefined. To solve this problem, we decided to describe the diethylmercury

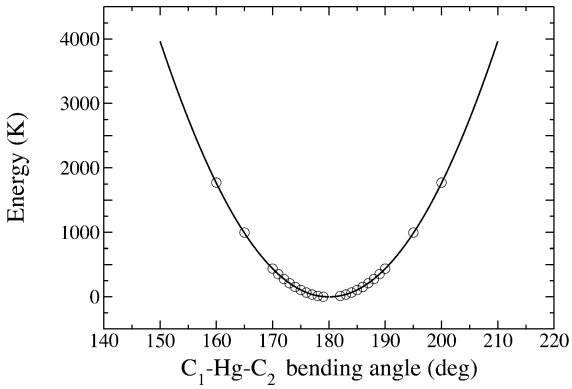

Figure 1. Energy of dimethylmercury as a function of the C−Hg−C bending angle from ab initio calculations. Circles: ab initio data. Continuous line: fit according to eq 3.

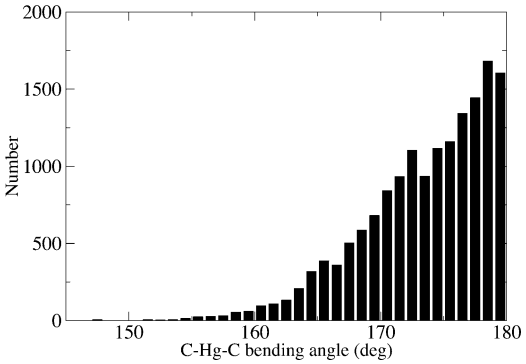

Figure 2. Distribution of the C−Hg−C bending angle of dimethylmercury during a Monte Carlo simulation of 10 million steps at 293.15 K.

TABLE 2: Bond Lengths, Bending, and *Supertorsion* Parameters for Dimethylmercury and Diethylmercury

distance (Å)	C−C		1.535
	C−Hg		2.086
bending	C−Hg−C (dimethylmercury)	θ_0 (deg)	180
		k_θ (K)	14100
	C_1-C_2-Hg (diethylmercury)	θ_0 (deg)	113.4
		k_θ (K)	23260
	C_2-Hg-C_3 (diethylmercury)	θ_0 (deg)	180
		k_θ (K)	17140
supertorsion	$C_1-C_2-C_3-C_4$ (diethylmercury)	a_1	24.132
		a_2	5.8523
		a_3	−64.119
		a_4	16.172
		a_5	70.393
		a_6	−6.5592

with the $C_1-C_2-C_3-C_4$ dihedral angle instead of the classical dihedral angle $C_1-C_2-Hg-C_3$. We employ the term *supertorsion* because this angle involves atoms separated by four bonds and not by three bonds as in a classical torsion. The a_j supertorsion parameters are shown in Table 2.

Preliminary Monte Carlo simulations have been performed in order to study the distribution of the different angles in diethylmercury at 293.15 K. It appears that the C_2-Hg-C_3 bending angle is most often larger than 170°. Thus, this angle will be frozen to 180° in further simulations. Concerning the supertorsion moves, their influence is expected to be weak due to the small value of the energy barrier (50 K, see Figure 3), compared to torsional barrier of alkanes (2500 K[22]). The distribution of the $C_1-C_2-C_3-C_4$ dihedral angle has been tested with two Monte Carlo simulations, with or without considering the supertorsion potential ($a_j \neq 0$ or $a_j = 0$, respectively). It appears that the values of the $C_1-C_2-C_3-C_4$ angle are almost

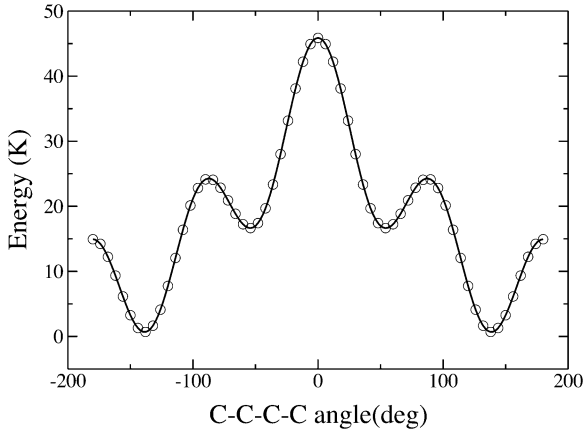

Figure 3. Energy of the diethylmercury as a function of the $C_1-C_2-C_3-C_4$ supertorsion angle from ab initio calculations. Circles: ab initio data. Continuous line: fit according to eq 4.

uniformly distributed between 0° and 180° and that there is no significant influence of the *supertorsion* potential. Thus we decided to let the $C_1-C_2-C_3-C_4$ angle free ($a_j = 0$ for all j).

To summarize, the bending angle of dimethylmercury is modeled either rigid ($k_\theta = 0$ and $\theta_0 = 180°$) or flexible ($k_\theta =$ 14100 K and $\theta_0 = 180°$). Concerning the diethylmercury, we have chosen to model the C_1-C_2-Hg bending angle flexible ($k_\theta = 23620$ K and $\theta_0 = 113.4°$), the C_2-Hg-C_3 bending angle rigid and linear ($k_\theta = 0$ and $\theta_0 = 180°$), and the $C_1-C_2-C_3-C_4$ supertorsion angle free ($a_j = 0$). However, since all bending angles have a high harmonic force constant, the C_1-C_2-Hg bending angle could be defined as rigid without changing the thermodynamic results.

3.3. Electrostatic Potential. Point charges are determined by the usual least-squares fit of the ab initio molecular potential on a grid of points.[7,8] The molecular potential was calculated at the MP2 level using the GAMESS package[23] with the same basis set as described in section 3.1. The grid of points, obtained using the point selection scheme of Singh and Kollman,[24] consists of a single shell of points located at two times the van der Waals radii, as it corresponds to the minimum distance for interpenetration of the electronic clouds. The density of points has been set to 1 point/Å^2. The root-mean-square (RMS) deviation and the relative root-mean-square (RRMS) deviation are used to estimate the accuracy of the fit.

Dimethylmercury. We first test four sets of point charges in the case of the linear conformation and with the methyl groups in a position out of line. The first set consists of the usual atomic charges (9 charges). The second one is composed of 3 charges, located on the mercury atom and on the two CH_3 AUA centers. The two last sets are obtained from the second one by adding 2 or 4 charges on the C−Hg−C axis (see Figure 4). The charges located on equivalent sites are constrained to be equal in the fitting procedure. The positions of the additional charges haven been chosen in order to minimize the resulting value of the RRMS deviation. The results are shown in Table 3. Atomic charges yield an accurate representation of the molecular potential (RRMS = 6%) on the fitting grid and a quadrupole moment in very good agreement with the MP2 value. This ensures a good representation of the molecular potential at short distances as well as at long distances. In the case of the three other sets the quadrupole moment is also very good. The accuracy at two times the van der Waals radii is significantly reduced but still reasonable (RRMS in the range 23−27%) so that we shall now restrain to the two smallest sets (3 and 5 charges) which are more consistent with the AUA model and less computer time-consuming.

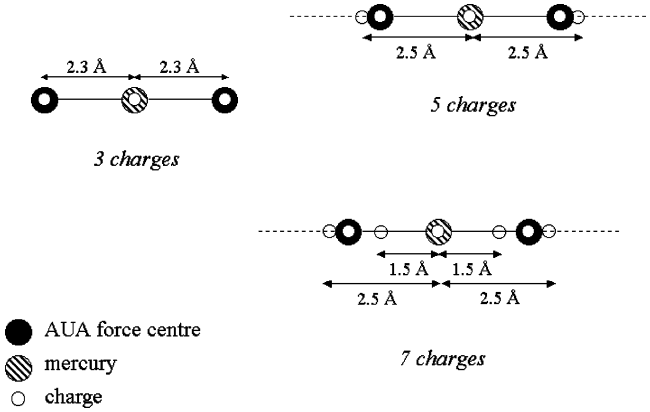

Figure 4. Charges location on the dimethylmercury.

We turn now to the problem of geometry-dependence of the charges. Two types of moves are to be considered: the rotation of methyl groups and the C−Hg−C bending. Ab initio calculations show that the methyl groups are free to rotate (this work, Rao et al.[21]), so that the effective electrostatic potential seen by another molecule is averaged over all the positions of these groups. Thus we proceed as follows: (i) for a given value of the C−Hg−C angle, we adjust the charges on a mean potential (referred hereafter as "mean methyl potential") obtained by averaging the values of the molecular potential of four conformations of the methyl groups, and (ii) we compare the charges obtained for different C−Hg−C angles and determine a unique set of charges. Specific fitting grids are needed for that part since we must calculate the electrostatic potential of conformations differing only by the positions of hydrogens on the same grid. We have used grids consisting of fused spheres centered on mercury, at two times the van der Waals radius, and on carbon, at a distance equal to the CH bond length plus two times the van der Waals radius of hydrogen.

Two values of the C−Hg−C bending angle were considered: $\theta = 180°$ (equilibrium value) and $\theta = 165°$ which corresponds to the wing of the distribution of the value of the C−Hg−C bending angle during a 10 million step Monte Carlo run (see Figure 2). With regard to the 3 charges set, the values of the charges obtained by fitting the mean potential differ by less than 2% between the two bending angles (this weak dependence is due to the small number of charges used here and to the absence of really buried atoms in the molecule). Thus we have simply taken the average values: $q_{Hg} = 0.204$ au, $q_{CH_3} = -0.102$ au. The calculation of the mean methyl potential using this set of charges leads to a reasonable accuracy: 16% for $\theta = 180°$ and 18% for $\theta = 165°$ (see Table 4). Concerning the 5 charges set, we first look for the best position of the additional charges. We impose two requirements in addition to the accuracy criteria: the additional charges should not be too far outside the AUA centers and their values should not depend too much on the bending angle. This leads to locate the additional charges at 0.45 Å outside of the AUA center. Proceeding in the same way as for the 3 charges model, we determine a unique 5 charges model (see Table 4) that fits the mean methyl potential with an accuracy in the range 9−13%, depending on the conformation.

Diethylmercury. Diethylmercury is represented in Figure 5, where the hydrogen atoms of the methyl groups are omitted. We studied two sets of charges. The first one, analogous to the 3 charges set used for dimethylmercury, consists of 5 charges (one on the mercury atom and one on each AUA center). The second one (7 charges) is obtained by adding one charge on

TABLE 3: Different Point Charges Models for the Linear Dimethylmercury[a]

no. of charges	charges values (au)					quadrupolar moment Q_{zz} (D·Å)	RMS (10^{-4} au)	RRMS (%)
	Hg	CH_3	H	q_{add1}	q_{add2}			
9	0.542	−0.769	0.166			−5.4	2.2	6
3	0.208	−0.104				−5.2	9.3	27
5	0.102	0.267		−0.318		−5.4	8.4	25
7	0.726	1.956		−0.889	−1.43	−5.6	7.8	23

[a] The set with 9 charges is the atomic charge set. q_{add1} is the additional charge outside of the CH_3 group, and q_{add2} is the additional charge inside of the CH_3 group. The *z* axis is the C−Hg−C axis. The MP2 value for Q_{zz} is −5.52 D·Å.

TABLE 4: 3 Charges and 5 Charges Models for Dimethylmercury[a]

	3 charges	5 charges
q_{Hg}	0.204	0.102
q_{CH_3}	−0.102	0.228
q_{add}		−0.279
RMS (180)	5	3
RRMS (180)	16	9
RMS (165)	6	5
RRMS (165)	18	13

[a] Values of charges are in au, RMS in 10^{-4} au, and RRMS in %. θ is the value of the C_2-Hg-C_3 bending angle. RMS(θ) and RRMS(θ) are related to the molecular potential averaged on the methyl conformations.

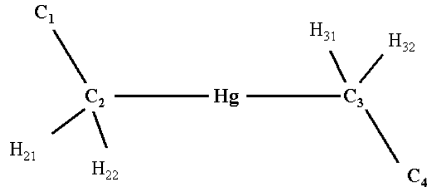

Figure 5. Schematic representation of the diethylmercury.

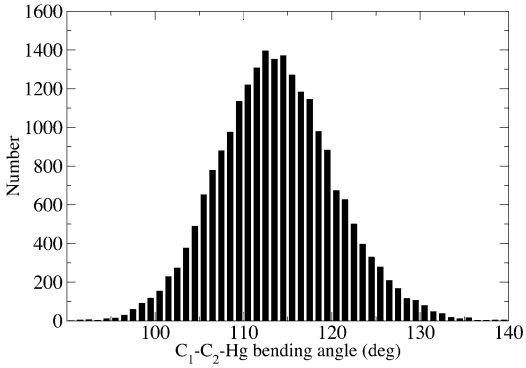

Figure 6. Distribution of the C_1-C_2-Hg bending angle of diethylmercury during a Monte Carlo simulation of 10 million steps at 293.15 K.

each CC bond, at 0.45 Å outside the AUA centers of the methyl groups: it is similar to the 5 charges set of dimethylmercury.

To be consistent with the intramolecular potential used for Monte Carlo simulations (see paragraph 3.2), we consider exclusively the equilibrium value of the C_2-Hg-C_3 angle (180°). Concerning the C_1-C_2-Hg bending, we consider 3 values, $\theta = 113.4°$ (equilibrium value), $\theta = 105°$, and $\theta = 120°$, which correspond to the mid height width of the distribution of this angle during a 10 million step Monte Carlo simulation (see Figure 6). For the *supertorsion*, we consider four regularly spaced values of the dihedral angle: $\phi = 0°$, 60°, 120°, 180°. Finally, we have performed ab initio calculations with a frozen $C_1-C_2-Hg-C_3-C_4$ skeleton and various conformations of the methyl groups. The results show a strong energy barrier of about 3500 K upon rotation of the methyl groups. Thus, for a given $C_1-C_2-Hg-C_3-C_4$ skeleton, we have only retained the molecular potential of the lowest energy conformation of the methyl groups when calculating the charges, in contrast with the case of the dimethylmercury, where an average potential was used to take into account the free character of the methyl rotation.

TABLE 5: 5 Charges and 7 Charges Models for Diethylmercury[a]

	5 charges	7 charges
q_{Hg}	0.184	0.176
q_{CH_2}	−0.071	−0.089
q_{CH_3}	−0.021	0.184
q_{add}		−0.183
RMS (180)	7.2	8
RRMS (180)	29−32	23−24

[a] Same units as in Table 4. RMS(180) and RRMS(180): range of the RMS and the RRMS deviations of the molecular potential for different values of the supertorsion angle when the C_2-Hg-C_3 bending angle is equal to 180°. The C_1-C_2-Hg bending angle and the position of the methyl groups result from the optimized geometry of the molecule.

We first calculate the values of the charges for the conformations corresponding to $\theta = 113.4°$ and to the four values retained for the supertorsion angle. When using the 5 charges set, it appears that the dependence of the charges on ϕ is weak (less than 10%). Averaging the values of the different sets leads to the results shown in Table 5. This averaged model represents the molecular potential with an accuracy in the range 29−32%. These values of RRMS are significantly larger than those obtained for linear dimethylmercury with the 3 charges set (16%). This is due to the fact that the organic part in diethylmercury is larger than in dimethylmercury, leading to lower values of the molecular potential (the root-mean-square values of the potential are respectively 0.0025 au and 0.0034 au). Thus the same absolute deviation (RMS) leads to a larger RRMS value in the case of diethylmercury. In addition the molecular potential to be fitted in the case of the dimethylmercury is averaged over conformations of the methyl groups, while the potential of one particular methyl conformation is used in the case of the diethylmercury. Thus, the charge model used here (point charges localized on Hg and on the CC bond axis) is more adapted in the case of dimethylmercury than in the case of diethylmercury. A better model for diethylmercury would require charges localized outside the CC bonds. Due to the weak values of the potential of diethylmercury, we did not investigate this eventuality. With regard to the 7 charges model, the same procedure as for the 5 charges model leads to a final averaged set that fits the molecular potential with an accuracy in the range 23−24% (see Table 5). Finally we have tested these two sets on the conformations with the C_1-C_2-Hg bending angle different from the equilibrium value. In every case, the RRMS is lower than 30%, indicating that these charge models are still reasonably accurate when the molecule is deformed.

3.4. Lennard-Jones Potential. As already mentioned, we use the Anisotropic United Atoms potentials (AUA4) of Ungerer et al.[9] for the CH_3 and CH_2 groups. The parameters of these

TABLE 6: Lennard-Jones Parameters of the CH_3 and the CH_2 Groups[9]

groups	σ (Å)	ϵ/k (K)	δ (Å)
CH_3	3.6072	120.15	0.21584
CH_2	3.4612	86.291	0.38405

TABLE 7: Experimental Data for Dimethylmercury and Diethylmercury

	thermodynamic properties		
dimethylmercury T (K)	ρ_{liquid}[10] (kg·m^{-3})	P_{sat} in kPa[11]	ΔH_{vap} (kJ·mol^{-1})[a]
261.95		1.2	36.2
273.95		2.4	35.6
281.15		3.5	35.3
293.15[c]	3022	7.8	34.8
308.95		13.6	34.2
324.85		25.7	33.2
337.15		40.7	33.3
358.25		81.0	32.7
375.15[c]		131.6[b]	
T_b = 365.15 K[11]			

	thermodynamic properties		
diethylmercury T (K)	ρ_{liquid}[10] (kg·m^{-3})	P_{sat} in kPa[12]	ΔH_{vap} (kJ·mol^{-1})[a]
293.15[c]	2466		
337.15[c]		3.7	
345.15[c]			40.7
353.15[c]		7.2	
T_b = 432.15 K[10]			

[a] These data are obtained by fitting a second-order polynomial function on the Clapeyron diagram. [b] Data derived from the extrapolation of the Clapeyron diagrams slightly above the boiling temperature. [c] Reference conditions for the optimization of the Lennard-Jones parameters.

potentials are given in Table 6, where the distance between the CH_3 or CH_2 force center and the carbon nucleus is represented by δ. In this work, we place the center of force corresponding to the mercury atom on the mercury nucleus, and we optimize its parameters σ_{Hg} and ϵ_{Hg}, following the procedure of Ungerer et al.,[9] considering dimethylmercury and/or diethylmercury as reference compounds. The thermodynamic experimental values used in the fitting procedure are given in Table 7.

We decided to optimize the Lennard-Jones parameters of the mercury atom without taking into account electrostatic interactions. A preliminary Monte Carlo simulation of liquid dimethylmercury (rigid and linear) at 293.15 K, using the Lennard-Jones parameters of mercury given in ref 25 (σ_{Hg} = 2.9 Å and ϵ_{Hg}/k = 800 K) and atomic charges, shows that the electrostatic energy represents 0.4% of the total energy, a very low contribution due to the weak polar character of dimethylmercury.

To get a better set of initial values of the mercury parameters (the parameters of ref 25 were adapted for gas viscosity calculations) we carried out ten Monte Carlo simulations with regularly spaced values of the mercury parameters, and we retained the ones which reproduce at best the liquid density at 293.15 K: σ_{Hg} = 3.68 Å and ϵ_{Hg}/k = 470.0 K.

A first set of parameters was optimized using reference data of dimethylmercury alone. The simulations were run without electrostatics and considering dimethylmercury linear and rigid. The result is shown in Table 8 (set I). A second set (set II, Table 8) was optimized using reference data of both dimethylmercury and diethylmercury. The small differences between the parameters of sets I and II indicate that the optimum Lennard-Jones parameters are well defined.

TABLE 8: Optimized Lennard-Jones Parameters of Dimethylmercury and Diethylmercury[a]

parameters set	reference compounds	σ_{Hg} (Å)	ϵ_{Hg}/k (K)
I	dimethylmercury	3.505	426.11
II	dimethylmercury and diethylmercury	3.547	442.28

[a] Dimethylmercury is considered rigid.

3.5. Thermodynamic Properties. *Dimethylmercury and Diethylmercury.* Monte Carlo simulations were run for dimethylmercury using the set I of Lennard-Jones parameters, for temperature in the range 275−400 K, with different models (rigid linear or flexible, including electrostatics or not). The liquid density, the vapor pressure, and the vaporization enthalpy are reported in Figures 7−9, respectively, together with the experimental data of Pascal[10] and Long et al.[11] Whatever the model, calculated values of the liquid density slightly overestimate the only available experimental value at 293.15 K (deviations smaller than 2%). The vapor pressure is very well reproduced except with the 3 charges model (errors in the range 10−20%). The vaporization enthalpy is slightly overestimated when electrostatic interactions are not taken into account and slightly underestimated for the three and five charges models, with deviations smaller than 0.4 kJ/mol. As the latter property is derived from vapor pressure measurements from a limited number of points, we may consider that the simulated vaporization enthalpies of dimethylmercury are consistent with experiment-based results within their uncertainty. These results show that the calculated thermodynamic properties are not significantly modified whether dimethylmercury is considered rigid or flexible, with or without electrostatic effects.

The set I of Lennard-Jones parameters was then applied to diethylmercury, without electrostatics, since the polar character of diethylmercury is even smaller than that of dimethylmercury. The results are shown in Figures 10−12. The only available experimental value of the liquid density, at 298.15 K, is well reproduced (calculated value: 2359 kg·m^{-3}, experimental value: 2466 kg·m^{-3}). Calculated values for vapor pressure are in qualitative agreement with experimental ones, with deviations of the order of 50%. At 345.15 K, the calculated vaporization energy (40.5 kJ·mol^{-1}) is in very good agreement with experiment (40.7 kJ·mol^{-1}).

The results using set II without electrostatics are also shown for both compounds in Figures 10−12. These values are compared with the corresponding experimental data of Pascal,[10] Long et al.,[11] and Thomson et al.[12] The set II of parameters provides a small improvement of vapor pressure description for diethylmercury (Figure 11), however not yet satisfactory. With the same set, the vaporization enthalpy of dimethylmercury is worse than with set I (Figure 12). It may be concluded that a fair qualitative prediction of diethylmercury is obtained with the dimethylmercury-based parameters (set I) and that the coupled optimization of the mercury atom parameters on both compounds (set II) is not sufficient to provide a quantitative agreement with experiments.

Dimethylmercury−n-Pentane Mixture. We have performed Monte Carlo simulations in the Gibbs ensemble (2 phases) at constant pressure at T = 400 K in order to establish the liquid−vapor diagram of the dimethylmercury−*n*-pentane mixture in a purely predictive way. The set I (Table 8) of Lennard-Jones parameters is used for dimethylmercury and the Lennard-Jones parameters of Ungerer et al.[9] for *n*-pentane (Table 6). Figure 13 represents the pressure versus composition (P,x) phase diagram. The end points (i.e. when the molar fraction is equal

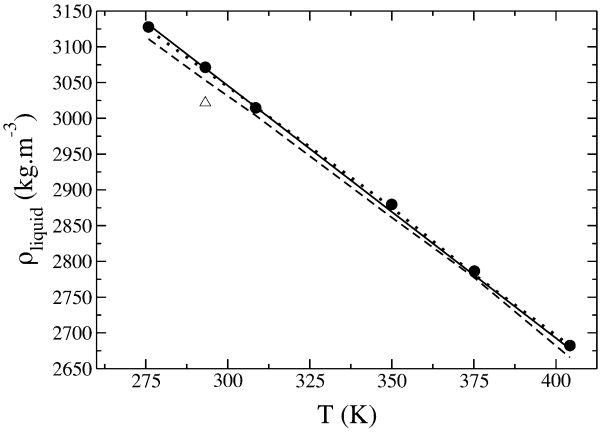

Figure 7. Monte Carlo simulation results for dimethylmercury liquid density, using parameter set I, in the case of four models: rigid, linear, and without electrostatic interactions (—); rigid, linear, and 3 charges (- -); rigid, linear, and 5 charges (···); flexible and without electrostatic interactions (●), compared with the experimental data (△) of Pascal.[10]

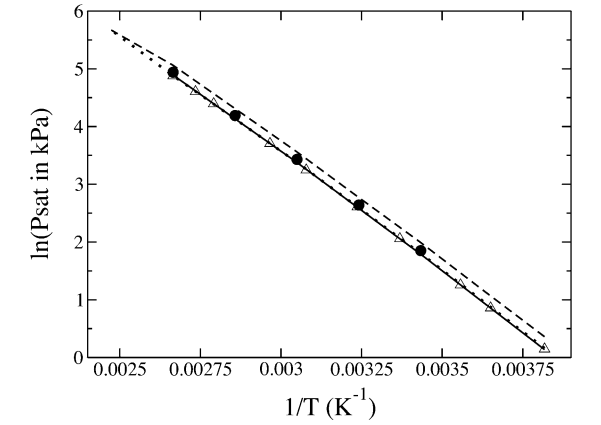

Figure 8. Monte Carlo simulation results for dimethylmercury vapor pressure, using parameter set I, in the case of four models: linear, rigid, and without electrostatic interactions (—); rigid, linear, and 3 charges (- -); rigid, linear, and 5 charges (···); flexible and without electrostatic interactions (●), compared with the experimental data (△) of Long et al.[11]

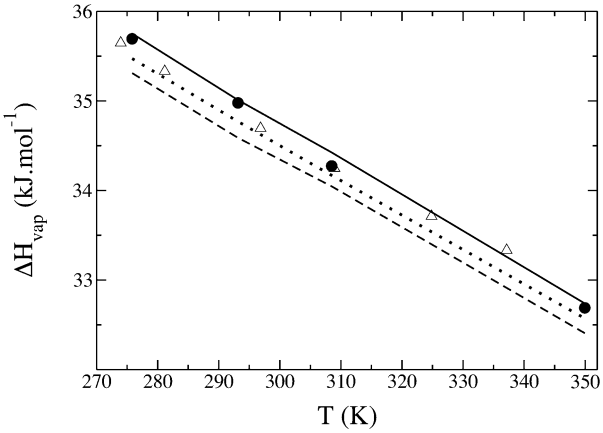

Figure 9. Monte Carlo simulation results for dimethylmercury vaporization enthalpy, using parameter set I, in the case of four models: linear, rigid, and without electrostatic interactions (—); rigid, linear, and 3 charges (- -); rigid, linear, and 5 charges (···); flexible and without electrostatic interactions (●), compared with the data (△) derived from the Clapeyron diagram of Long et al.[11]

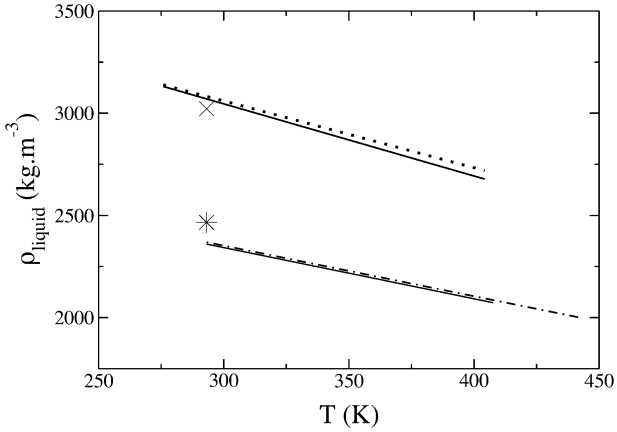

Figure 10. Liquid density of dimethylmercury and diethylmercury without electrostatics, using either set I or set II for Lennard-Jones parameters (Table 8), compared with the experimental data of Pascal.[10] Dimethylmercury: experimental (×), set I (—), set II (- -). Diethylmercury: experimental (∗), set I (—), set II (— - —).

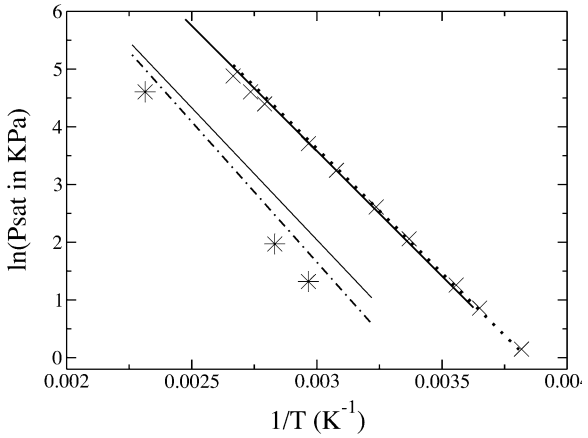

Figure 11. Vapor pressure of dimethylmercury and diethylmercury without electrostatics, using either set I or set II for Lennard-Jones parameters (Table 8), compared respectively with the experimental data of Long et al.[11] and Thomson et al.[12] Dimethylmercury: experimental (×), set I (—), set II (- -). Diethylmercury: experimental (∗), set I (—), set II (— - —).

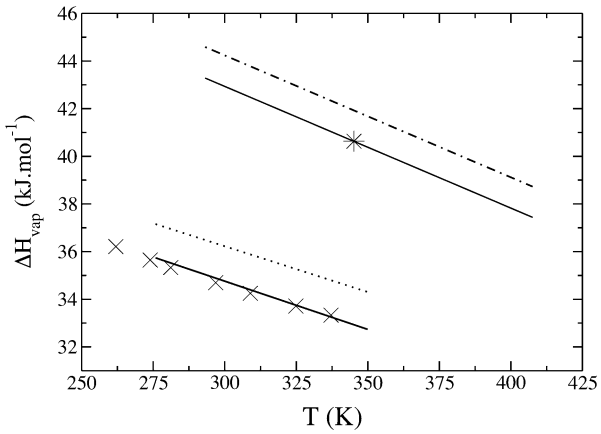

Figure 12. Vaporization enthalpy of dimethylmercury and diethylmercury without without electrostatics, using either set I or set II for Lennard-Jones parameters (Table 8), compared respectively with the data derived from the Clapeyron diagram of Long et al.[11] and Thomson et al.[12] Dimethylmercury: experimental (×), set I (—), set II (- -). Diethylmercury: experimental (∗), set I (—), set II (— - —).

to 0 or 1) are obtained with simulations in the Gibbs ensemble at constant volume for the pure compounds. For pressures close to the saturation pressure of dimethylmercury—i.e., in the lower part of the (P,x) diagram—we observe a persisting difference in composition between the liquid and the vapor phases. This indicates the existence of an azeotrope for a molar fraction of

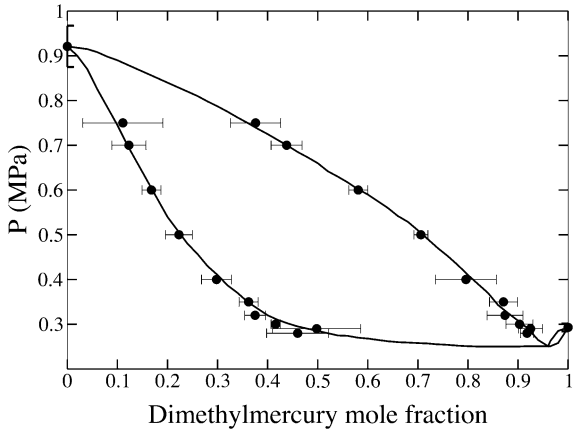

Figure 13. Dimethylmercury−*n*-pentane liquid−vapor diagram at $T = 400$ K. ●: Monte Carlo results. —: tendency curves.

dimethylmercury of $x = 0.95$. This kind of azeotrope with a minimum in a (P,x) diagram is less frequent than maximum azeotropes but is nevertheless also observed.[26]

4. Conclusion

We performed ab initio calculations and Monte Carlo simulations in order to derive a complete force field for two organic mercury compounds: dimethylmercury and diethylmercury. It required significant adaptation compared to similar studies[5,6] because of a lack of experimental thermodynamic properties for the adjustment and because of the peculiar structure of organic mercury compounds.

Dimethylmercury can be considered either with a rigid C−Hg−C angle of 180° or flexible with a rigidity constant of $k_\theta = 14100$ K. In the case of diethylmercury, we introduce a free *supertorsion* to define the dihedral behavior of the four carbon atoms.

As far as the electrostatic interactions are concerned, we chose specific distributions of the electrostatic sites for which the values of charges are fitted to reproduce at best the ab initio molecular electrostatic potential. Two sets of charges have been determined for each molecule, leading to a representation of the molecular electrostatic potential with an accuracy in the range 10−30%, depending of the molecular and of the conformation (position of the methyl groups, bending and *supertorsion* angle). From Monte Carlo simulations in the liquid phase of pure dimethylmercury or diethylmercury, we found that the electrostatic intermolecular interactions represent a small part of the total energy (0.4%), so that there is no need to introduce electrostatics for pure liquids.

By fitting the Lennard-Jones parameters of the mercury atom on available thermodynamic properties (liquid density, vapor pressure, and vaporization enthalpy) of the two compounds, we determined two sets of parameters which are a function of the reference compounds taken into account in the optimization. These parameters give results in sensible agreement with the few available experimental data. The set of parameters optimized for dimethylmercury, rigid, linear, and without electrostatics ($\sigma_{Hg} = 3.505$ Å and $\epsilon_{Hg} = 426.11$ K) can be used to calculate the thermodynamic properties of this molecule when it is flexible and/or including electrostatics, without significant changes in the results. This set enables us to predict the liquid−vapor diagram of the dimethylmercury−*n*-pentane mixture and to observe a light minimum azeotrope. However the proposed model is still insufficient to provide quantitative descriptions for diethylmercury, which is not surprising considering the simplicity of the Lennard-Jones potential. The simultaneous representation of dimethylmercury and diethylmercury would probably require a different form of the intermolecular potential such as the exponential-6 model.[27] This model involves indeed three parameters, which makes it more flexible than the Lennard-Jones potential to fit the thermodynamical behavior. The prediction of other phase diagrams involving organic mercury compounds, particularly with polar solvents, is a promising research avenue where the account of electrostatic interactions could be evaluated.

Acknowledgment. The authors thank F. Montel and H. Zhou from Total, V. Ruffier-Meray from the Institut Français du Pétrole, and S. Degrange-Meunier from Gaz de France for their helpful comments and P. Archirel from LCP for his help with the ab initio calculations.

References and Notes

(1) Snell, J. P.; Frech, W.; Thomassen, Y. *Analyst* **1996**, *121*, 1055.

(2) Snell, J. P.; Qian, J.; Johansson, M.; Smit, K.; Frech, W. *Analyst* **1998**, *123*, 905.

(3) Shiowatana, J.; Siripinyanond, A.; Waiyawat, W.; Nilmanee, S. *At. Spectrosc.* **1999**, *20*, 224.

(4) Spirié, Z.; Mashyanov, N. R. *Fresenius J. Anal. Chem.* **2000**, *366*, 429.

(5) Delhommelle, J.; Tschirwitz, C.; Ungerer, P.; Granucci, G.; Millié, P.; Pattou, D.; Fuchs, A. H. *J. Phys. Chem.* **2000**, *104*, 4745.

(6) Kranias, S.; Pattou, D.; Lévy, B.; Boutin, A. *Phys. Chem. Chem. Phys.* **2003**, *5*, 4175.

(7) Cox, S. R.; Williams, D. E. *J. Comput. Chem.* **1981**, *2*, 304.

(8) Lévy, B.; Enescu, M. *J. Mol. Struct.* **1998**, *432*, 235.

(9) Ungerer, P.; Beauvais, C.; Delhommelle, J.; Boutin, A.; Rousseau, B.; Fuchs, A. H. *J. Chem. Phys.* **2000**, *112*, 5499.

(10) Pascal, P. *Nouveau traité de chimie minérale − Combinaisons organo-mercuriques*; Masson et C^{ie}, 1957; Vol. V, pp 901−951.

(11) Long, L. H.; Cattanach, J. *J. Inorg. Nucl. Chem.* **1961**, *112*, 5499.

(12) Thomson, H. W.; Linnett, J. W. *Trans. Faraday Soc.* **1936**, *32*, 681.

(13) Toxvaerd, S. *J. Chem. Phys* **1997**, *107*, 5197.

(14) Allen, M. P.; Tildesley, D. J. *Computer Simulation of Liquids*; Oxford Science Publication: Oxford, 1987.

(15) Panagiotopoulos, A. *Mol. Sim.* **1987**, *61*, 813.

(16) Smit, B.; Karaborni, S.; Siepmann, J. I. *J. Chem. Phys.* **1995**, *102*, 2126.

(17) Bourasseau, E.; Ungerer, P.; Boutin, A.; Fuchs, A. H. *Mol. Sim.* **2002**, *75*, 363.

(18) Kofke, D. A. *J. Chem. Phys.* **1993**, *98*, 4149.

(19) Gaussian 98, Revision A.6. Frisch, M. J.; Trucks, G. W.; Schlegel, H. B.; Scuseria, G. E.; Robb, M. A.; Cheeseman, J. R.; Zakrzewski, V. G.; Montgomery, J. A., Jr.; Stratmann, R. E.; Burant, J. C.; Dapprich, S.; Millam, J. M.; Daniels, A. D.; Kudin, K. N.; Strain, M. C.; Farkas, O.; Tomasi, J.; Barone, V.; Cossi, M.; Cammi, R.; Mennucci, B.; Pomelli, C.; Adamo, C.; Clifford, S.; Ochterski, J.; Petersson, G. A.; Ayala, P. Y.; Cui, Q.; Morokuma, K.; Malick, D. K.; Rabuck, A. D.; Raghavachari, K.; Foresman, J. B.; Cioslowski, J.; Ortiz, J. V.; Stefanov, B. B.; Liu, G.; Liashenko, A.; Piskorz, P.; Komaromi, I.; Gomperts, R.; Martin, R. L.; Fox, D. J.; Keith, T.; Al-Laham, M. A.; Peng, C. Y.; Nanayakkara, A.; Gonzalez, C.; Challacombe, M.; Gill, P. M. W.; Johnson, B.; Chen, W.; Wong, M. W.; Andres, J. L.; Gonzalez, C.; Head-Gordon, M.; Replogle, E. S.; Pople, J. A. Gaussian, Inc.: Pittsburgh, PA, 1998.

(20) Stevens, W. J.; Basch, H.; Krauss, M. *J. Chem. Phys.* **1984**, *81*, 6026. Stevens, W. J.; Krauss, M.; Basch, H.; Jasien, P. G. *Can. J. Chem.* **1992**, *70*, 612. Cundari, T. R.; Stevens, W. J. *J. Chem. Phys.* **1993**, *98*, 5555.

(21) Rao, K. S.; Stoïcheff, B. P.; Turner, R. *Can. J. Phys.* **1960**, *38*, 1516.

(22) Toxvaerd, S. *J. Chem. Phys.* **1990**, *93*, 4290.

(23) Schmidt, M. W.; Baldridge, K. K.; Boatz, J. A.; Elbert, S. T.; Gordon, M. S.; Jensen, J. H.; Koseki, S.; Matsunaga, N.; Nguyen, K. A.; Su, S. J.; Windus, T. L.; Dupuis, M.; Montgomery, J. A. *J. Comput. Chem.* **1993**, *14*, 1347.

(24) Singh, U. C.; Kollman, P. A. *J. Comput. Chem.* **1984**, *5*, 129.

(25) Rowley, R. L. *Statistical mechanics for thermophysical property prediction*; Prentice Hall: 1994.

(26) Vidal, J. *Thermodynamique, Application au génie chimique et à l'industrie pétrolière*; Technip, 1997.

(27) Errington, J. R.; Panagiotopoulos, A. Z. *J. Chem. Phys.* **1998**, *109*, 1093.